The 2014 World Congress on
Advances in Civil, Environmental, and Materials Research (ACEM14)
Busan, Korea, August 24-28, 2014

Chemical Synthesis of Cr doped Iron Oxide Nanoparticles

*Saira Riaz [1)] and Shahzad Naseem[2)]

[1), 2)] *Centre of Excellence in Solid State Physics, University of the Punjab, Lahore 54590, Pakistan*

[1)] saira_cssp@yahoo.com

ABSTRACT

Amongst various phases of iron oxide, hematite (α-Fe_2O_3) has attracted world attraction due wide range of technological and industrial applications including spintronic and data storage devices. However hematite exhibits weak ferromagnetic behavior at room temperature. For enhancing the magnetic properties of hematite nanoparticles we here report structural and magnetic properties of Cr doped Fe_2O_3 nanoparticles prepared using sol-gel method. The dopant concentration is varied as 2%, 4%, 6%, 8% and 10%. The nanoparticles are characterized using Bruker D8 Advance X-ray Diffractometer (XRD) and Lakeshore's 7407 Vibrating Sample Magnetometer (VSM). Presence of (012), (104), (110), (113), (024), (116), (214) and (300) planes in XRD indicate the formation of Fe_2O_3 phase. XRD results indicate that incorporation of chromium causes contraction in unit cell that shifts the peak positions to higher diffraction angles. Undoped iron oxide nanoparticles show weak ferromagnetic behavior because of the presence of uncompensated magnetic moments between two sublattice that give rise to canting of spin structure. Incorporation of chromium in the host hematite lattice leads to appearance of localized magnetic moments in hematite nanoparticles thus leading to increase in magnetic properties. At high dopant concentration, Cr atoms can go to the interstitial positions thus, possibility of having free Cr atoms at high dopant concentration lead to the distortion of magnetic behavior.

1. INTRODUCTION

Interest in transition metal oxides exhibiting unique electric and magnetic properties arises due to their wide applications in spintronic devices (Frydrych 2010. Rozun 2011). Among various metal oxides iron oxide hematite α-Fe_2O_3 is a promising candidate owing to its wide applications as a catalyst, optical and magnetic devices and most importantly in spintronic devices including magnetic tunnel junctions, spin transistors etc (Akbar 2014(a), Riaz 2014(a,b)). α-Fe_2O_3 is inexpensive and abundant in nature with semiconducting properties exhibiting a band gap of 2.2eV. Its unit cell can be

[1)] Professor

described as hexagonal with six formula units and lattice parameters a=5.03Å and c=13.75Å or it can be described as rhombohedral with two formula units and lattice parameters as a=5.43Å and α=55˚ (Rivera 2012, Varshney 2013, Lian 2012). The lattice is made up of hexagonal close pack oxygen anions with every four of six octahedral sites occupied by iron cations. Hematite is antiferromagnetic in nature with Neel temperature of 955K exhibiting insulating properties. Below temperature of 260K shows a transition from antiferromagnetic to weak ferromagnetic behavior. This transition in magnetic properties arises due to canting in the magnetization of two sublattices in hematite crystal structure (Yogi 2013, Suresh 2012).

Due to spin orbit coupling canting between two adjacent planes arises that produces uncompensated magnetic moment of Fe^{3+} cations. Thus, weak ferromagnetic or canted ferromagnetic behavior arises in otherwise antiferromagnetic hematite. As the temperature is reduced below 260K the spin direction of (111) planes changes from in plane to out of plane thus resulting in completely parallel arrangement of spins in the same plane while perfectly antiparallel coupling arises with the spins of adjacent planes thus converting hematite from weak ferromagnetic to antiferromagnetic. This type of transition is known as Morin Transition. The main controlling parameters of Morin transition are anisotropy energy constant and superexchange interaction in Fe^{3+}-O-Fe^{3+} system (Rivera 2012, Garcia 2008 Akbar 2014(b)).

In order to improve the magnetic properties of hematite doping of various cations has been reported in literature including Co, Cr, Zn, Mg etc. based on the valence state as well as ionic radius. Trivalent cations are most important in this regard. For this purpose we here report the preparation and characterization of chromium doped iron oxide nanoparticles (NPs) prepared using sol-gel method. The dopant concentration is varied as 2-10%.

2. EXPERIMENTAL DETAILS

Cr doped α-Fe_2O_3 NPs were prepared using sol-gel method. Iron nitrate $Fe(NO_3)_3.9H_2O$ was used as precursor and ethylene glycol and water as the solvent. Iron nitrate was dissolved in DI water. Ethylene glycol was added to the above solution. The solution was heated on hotplate at 60˚C to obtain stable sol. The details of sol-gel synthesis are reported earlier (Akbar 2014). For Cr doped α-Fe_2O_3, $CrCl_3.6H_2O$ was dissolved in deionized water and added to iron oxide sol. The dopant concentration is varied as 2%-10%. For NPs synthesis, the reaction was carried out at 80˚C on hot plate.

Structural characterization of chromium doped iron oxide NPs was carried out using Bruker D8 Advance X-ray diffrcatometer using λ=1.5406Å. Room temperature magnetic properties of chromium doped iron oxide nanoparticles were studied with the help of Lakeshore's 7407 Vibrating Sample Magnetometer.

3. RESULTS AND DISCUSSION

Fig. 1 shows XRD pattern for undoped iron oxide nanoparticles prepared using sol-gel method. The presence of diffraction peaks corresponding to planes (102), (104), (110), (113), (024), (116), (214) and (300) indicate the formation of pure hematite phase. XRD patterns of chromium doped iron oxide nanoparticles can be seen in Fig.

2. No peaks corresponding to chromium and/or chromium oxide were observed indicative of successful incorporation of chromium in iron oxide lattice. The shift of peak position, belonging to plane (202), to high diffraction angle is due to smaller ionic radius of chromium as compared to that of iron. This will lead to shrinkage of unit cell thus leading to decrease in *d*-spacing. This in turn will result in shift of peak positions to high angles.

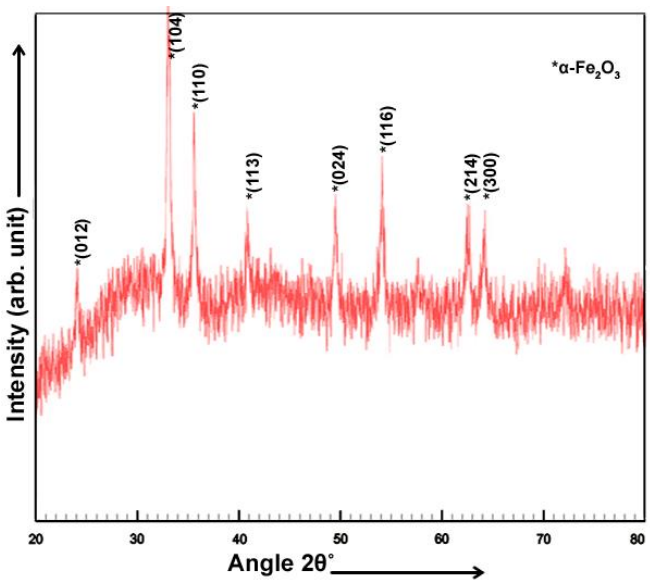

Fig. 1 XRD pattern for undoped iron oxide nanoparticles

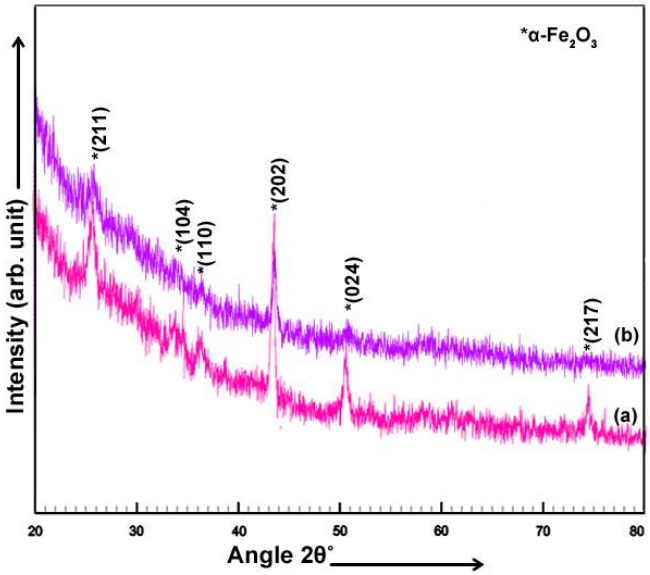

Fig. 2 XRD patterns for chromium doped iron oxide nanoparticles (a) 6% (b) 10%

Crystallite size (*t*) and dislocation density (*δ*) (Cullity 1956) of chromium doped iron oxide nanoparticles was calculated using Eq. (1)-(2)

$$t = \frac{0.9\lambda}{B\cos\theta} \quad (1)$$

$$\delta = \frac{1}{t^2} \quad (2)$$

Where, λ is the wavelength (1.5406Å), B is the Full Width at Half Maximum (FWHM). Crystallite size and dislocation density are plotted as a function of dopant concentration in Fig. 3. Crystallite size increases from 23nm for undoped iron oxide nanoparticles to 38.7nm for 6% doping concentration. Further increase in dopant concentration to 10% resulted in decrease in crystallite size to 25.87nm. Decrease in crystallite size at dopant concentration of 10% can be attributed to presence of amorphous impurities at the grain boundaries that increases the dislocation density to 14.9×10^{14} lines/m^2. As the result of presence of amorphous impurities at grain boundaries the reduction in crystallite size was observed.

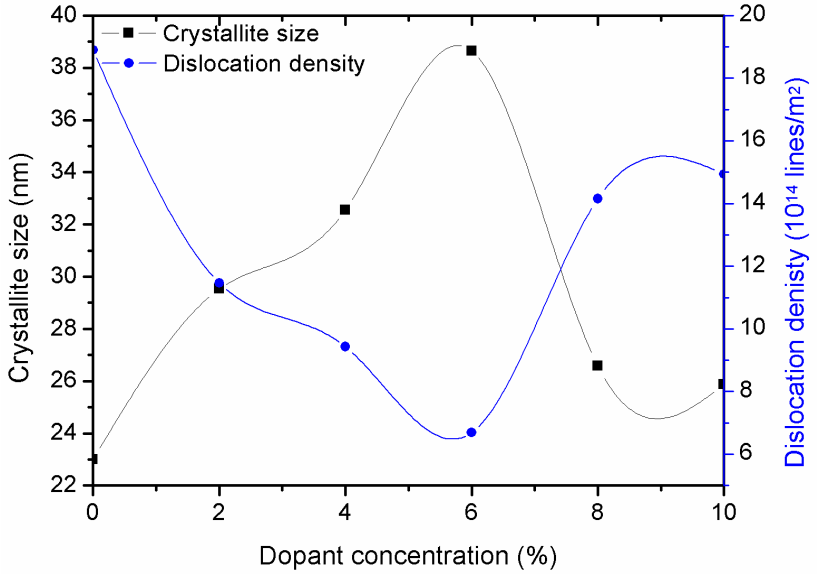

Fig. 3 Crystallite size and dislocation density as a function of dopant concentration

Lattice parameter and x-ray density of chromium doped iron oxide nanoparticles was calculated using Eq. 3 and 4 and are plotted as function of dopant concentration in Fig. 4. The decrease in lattice parameters and unit cell volume was observed with increase in dopant concentration due to smaller ionic radius of cobalt as compared to that of iron. Shrinkage of the unit cell was observed with increasing dopant concentration that leads to reduction in lattice parameters *a* and *c*.

$$\sin^2\theta = \frac{\lambda^2}{3a^2}\left(h^2 + k^2 + hk\right) + \frac{\lambda^2 l^2}{4c^2} \quad (1)$$

$$\rho = \frac{1.66042\,\Sigma A}{V} \quad (2)$$

Where, *(hkl)* represent the miller indices, *ΣA* is the sum of atomic weights of the

atoms in the unit cell, V is the volume of unit cell (V=0.866a^2c).

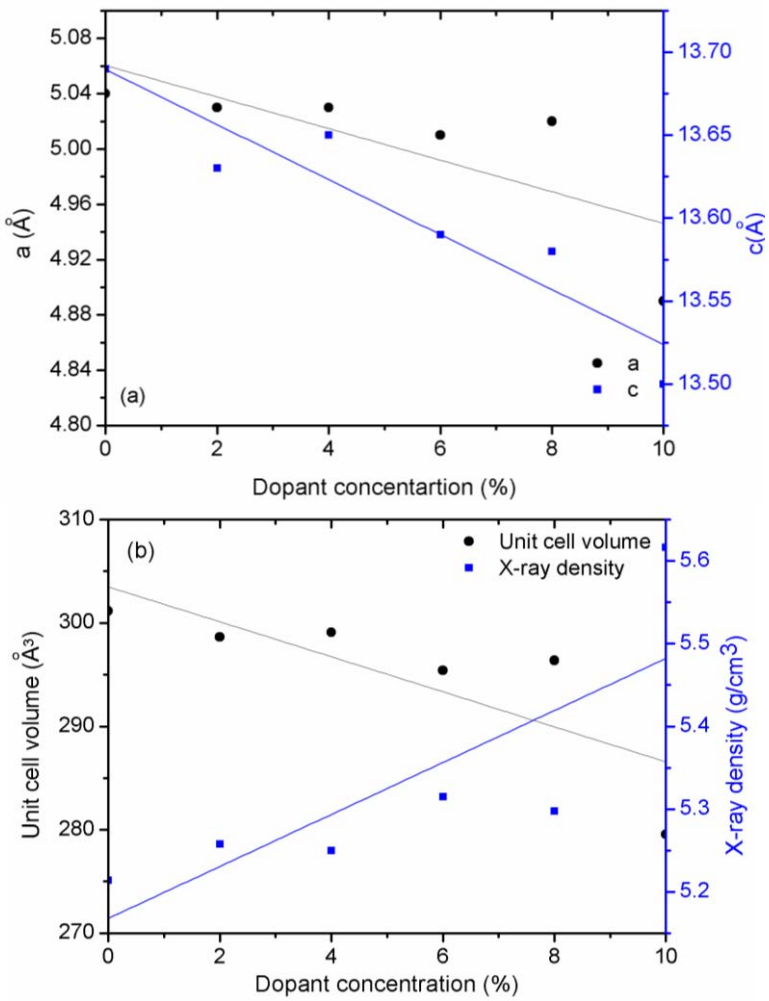

Fig. 4 (a) Lattice parameter (b) unit cell volume and x-ray density as a function of dopant concentration

Fig. 5 show M-H curves for chromium doped iron oxide nanoparticles. The nanoparticles show ferromagnetic behavior. Saturation magnetization and coercivity of chromium doped hematite nanoparticles are plotted as a function of dopant concentration in Fig. 6. In case of hematite, the spins in the same plane are ferromagnetically coupled. Spins in adjacent planes have antiferromagnetic alignment with each other. Antiferromagnetic coupling arises with the spins of the adjacent planes. Spin orbit coupling between the two adjacent planes give rise to uncompensated spins of Fe^{3+} cations (Akbar 2014, Rivera 2012). These uncompensated spins (Riaz 2011, Rivera 2012) produce the canting of spins between the planes. This is the cause of ferromagnetic behavior in otherwise antiferromagnetic hematite. Tremendous increase in saturation magnetization is observed with increase in dopant concentration to 6%. The incorporation of chromium in the host hematite lattice leads to presence of localized magnetic moments. Iron atom has a magnetic moment approximately equal to 4μB. But, due to antiparallel arrangement of the spins in hematite antiferromagnetic

behavior arises in hematite. It converts to weak ferromagnetic due to canting of spin structure (Akbar 2014, Rivera 2012). The introduction of foreign atoms produced perturbations in hematite that leads to changes in magnetic properties.

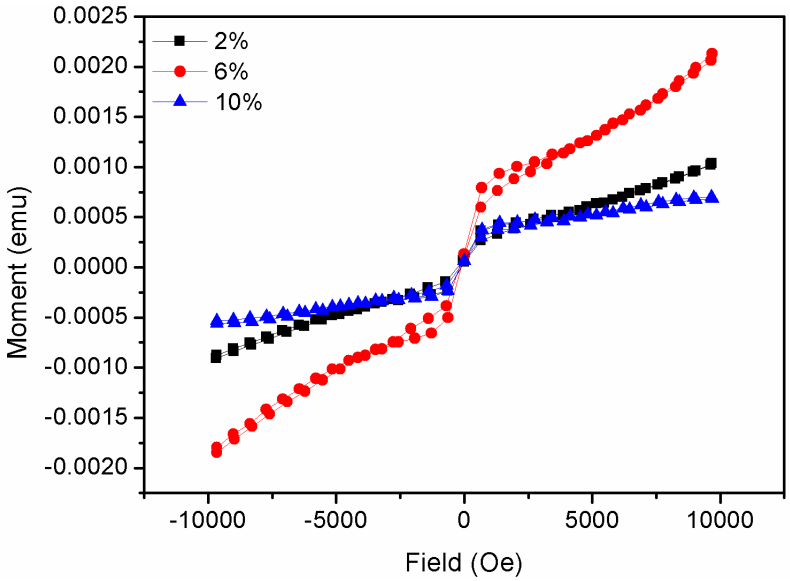

Fig. 5 M-H curves for chromium doped iron oxide nanoparticles

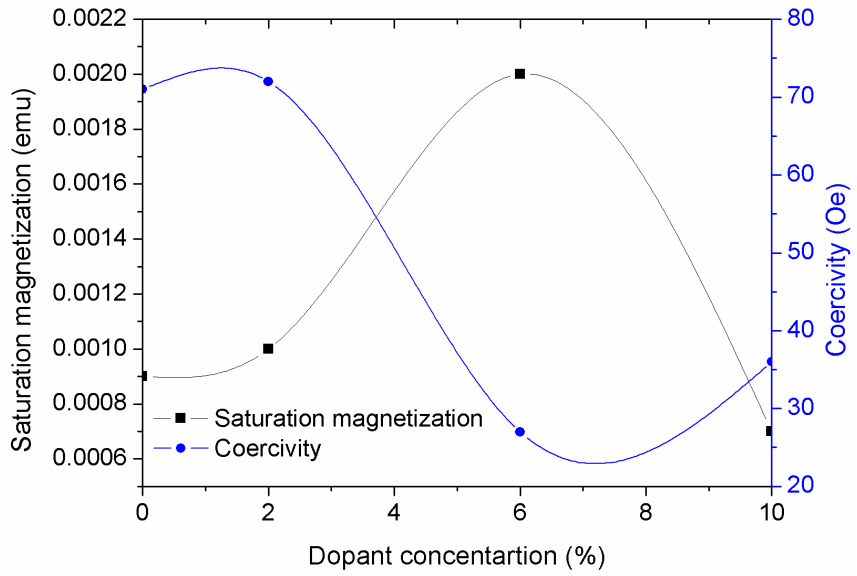

Fig. 6 Saturation magnetization and coercivity as a function of dopant concentration

4. CONCLUSIONS

Chromium doped iron oxide nanoparticles were prepared using sol-gel method. The presence of diffraction planes (102), (104), (110), (113), (024), (116), (214) and (300) indicated the formation of pure hematite phase. Effect of dopant concentration on

structural parameters indicated the successful incorporation of chromium in host lattice. Variation in lattice parameters and unit cell volume arises due to difference in ionic radius of chromium and iron. Chromium doped iron oxide NPS show ferromagnetic behavior and saturation magnetization increases as dopant concentration was increased to 6%. Ferromagnetic behavior in chromium doped iron oxide NPS arises due to perturbations produced in the host lattice.

REFERENCES

Akbar, A., Riaz, S., Bashir, M. and Naseem, S. (2014(a)), "Effect of Fe^{3+}/Fe^{2+} ratio on superparamagnetic behaviour of spin coated iron oxide thin films," *IEEE Trans. Magn.*, doi: 10.1109/TMAG.2014.2312972.

Akbar, A., Riaz, S., Ashraf, R. and Naseem, S. (2014(b)), "Magnetic and magnetization properties of Co-doped Fe_2O_3 thin films," *IEEE Trans. Magn.*, doi: 10.1109/TMAG.2014.2311826

Cullity, B.D. (1956), "Elements of x-ray diffraction," Addison Wesley Publishing Company, USA.

Frydrych, J., Machala, L., Hermanek, M., Medrik, I., Mashlan, M., Tucek, J., Pechousek, J. and Sharma, V.K. (2010), "A nanocrystalline hematite film prepared from iron(III) chloride precursor," *Thin Solid Films*, **518**, 5916–5919

Garcia, H.A., Melo Jr., R.P., Azevedo, A. and Araujo, C.B. (2013), "Optical and structural characterization of iron oxide and cobalt oxide thin films at 800 nm," *Appl. Phys. B.*, **111**, 313-321

Glasscock, J.A., Barnes, P.R.F., Plumb, I.C., Bendavid, A. and Martin, P.J. (2008), "Structural, optical and electrical properties of undoped polycrystalline hematite thin films produced using filtered arc deposition," *Thin Solid Films*, **516**, 1716-1724.

Lian, X., Yang, X., Liu, S., Xu, Y., Jiang, C., Chen, J. and Wang, R. (2012), "Enhanced photoelectrochemical performance of Ti-doped hematite thin films prepared by the sol–gel method," *Appl. Surf. Sci.*, **258**, 2307– 2311

Pozun, Z.D. and Henkelman, G. (2011) "Hybrid density functional theory band structure engineering in hematite," *J. Chem. Phys.*, **134**, 224706

Riaz, S., Akbar, A. and Naseem, S. (2013), "Structural, electrical and magnetic properties of iron oxide thin films," *Adv. Sci. Lett.*, **19**, 828-833.

Riaz, S., Akbar, A. and Naseem, S. (2014(a)), "Controlled nanostructuring of multiphase core-shell iron oxide nanoparticles," *IEEE Trans. Magn.*, **50**, 2300204

Riaz, S., Bashir, M. and Naseem, S. (2014(b)), "Iron Oxide Nanoparticles Prepared by Modified Co-Precipitation Method," *IEEE Trans. Magn.*, **50**, 4003304

Rivera, R., Pinto, H.P., Stashans, A. and Piedra, L. (2012), "Density functional theory study of Al-doped hematite," *Phys. Scr.*, 85, 015602

Suresh, R., Prabu, R., Vijayaraj, A., Giribabu, K., Stephen, A. and Narayanan, V. (2012), "Facile synthesis of cobalt doped hematite nanospheres: Magnetic and their electrochemical sensing properties," *Mater. Chem. Phys.*, **134**, 590-596

Valdes, A.H., Zarate, R.A., Martinez, A.I., Canul, M.I.P., Lobato, M.A.G. and Villaroel, R. (2014), "The role of solvents on the physical properties of sprayed iron oxide films," *Vacuum*, **105,** 26-32

Varshney, D. andYogi, A. (2013), “Influence of Cr and Mn substitution on the structural and spectroscopic properties of doped hematite: α-$Fe_{2-x}M_xO_3$ (0.0≤x≤0.50),” *J. Molecular Structure*, **1052**, 105–111

Yogi, A. and Varshney, D. (2013), “Magnetic and structural properties of pure and Cr-doped hematite: α-$Fe_{2-x}Cr_xO_3$ ($0 \leq x \leq 1$),” *J. Adv. Ceram.*, **2**, 360-369